Hindawi
Mathematical Problems in Engineering
Volume 2018, Article ID 3545423, 14 pages
https://doi.org/10.1155/2018/3545423

Research Article

The Coupled Control of Floor Heave Based on a Composite Structure Consisting of Bolts and Concrete Antiarches

Wenxiang Zheng[1], **Yanlin Zhao**[2] **and Qingwei Bu**[1]

[1]*Institute of Mining and Coal, Inner Mongolia University of Science and Technology, Baotou, Inner Mongolia 014010, China*
[2]*Hunan Provincial Key Laboratory of Safe Mining Techniques of Coal Mines, Work Safety Key Lab on Prevention and Control of Gas and Roof Disasters for Southern Coal Mines, Hunan University of Science and Technology, Xiangtan, Hunan 411201, China*

Correspondence should be addressed to Yanlin Zhao; yanlin_8@163.com

Received 25 May 2018; Revised 7 August 2018; Accepted 13 August 2018; Published 27 August 2018

Academic Editor: Shailesh I. Kundalwal

A composite structure, including concrete antiarches and bolts, was designed to control the floor heave. This semiclosed structure may reinforce the floor and the two bottom corners of the roadway. Then, based on some relative assumptions, we established a model for this structure. We further analyzed this model and revealed the floor heave mechanism. In addition, based on the above analysis, we proposed the stability criterion for this structure. Moreover, with the practical conditions, we proposed a support system for the #1 roadway in S6 mining area of Changcun mine. Furthermore, the stability analysis and the numerical simulation verified the correctness of the design parameters. Simultaneously, the field investigation shows that the floor heave has been reduced by 78.7%, a close value to the mechanical analysis.

1. Introduction

To properly control the floor heave, extensive studies have proposed many control technologies [1–6], including the reinforcement method, the pressure relief method, and the combined (composite) support method [7–12]. In Guo et al. study [13], in order to propose highly efficient and economical methods of controlling floor heave, numerical simulation, laboratory physical simulation, and engineering practice were carried out to reveal the mechanism of reinforcing roof and sidewalls to control the floor heave of the mining roadway, and engineering practice showed that the floor heave in the roadway, the roof, and the sidewalls, which was reinforced by intensive bolts combined with steel belt, wire mesh, and cable, was significantly reduced compared with that with lower supporting intensity of roof and sidewalls. In Zhang et al. study [14], the dynamic distribution of the stress in the RGSG floor was examined to reveal the mechanism of floor heave. Finally, grouting reinforcement was proposed to control the RGSG floor, and the corresponding effectiveness was verified by improving the rock mechanics of the floor strata based on the results of numerical uniaxial compressive tests. In Li et al. study [5], based on the analysis of the mechanism of shear failure of the floor heave, the mechanical calculation model of the shear expansion heave is established, and the supporting force of the floor is discussed by the concrete engineering example. The numerical simulation of FLAC3D shows that the plastic failure zone of the roof and floor is significantly reduced, and the floor heave volume is also decreased. Hou et al. study [15], aimed at the serious problem of floor heave deformation in Dongyi auxiliaries transportation main roadway of Liujia coal mine, by using numerical simulation showed that scheme 2 (Bottom grouting (Three times grouting) + Cable beam (φ21.8 × 11000 mm) + Bottom beam) is the best scheme. In Liu et al. study [16], based on the floor heave mechanism in gob-side entry retaining, mechanical model of floor beam in gob-side entry retaining is established. By using the reciprocal theorem, the deflection formula of floor in gob-side entry retaining is derived. The calculated result shows that calculated deflection curve is in accordance with the deformation characteristics of roadway in gob-side entry retaining. The calculated result also shows that the maximum deformation of the floor increases with the increase of the

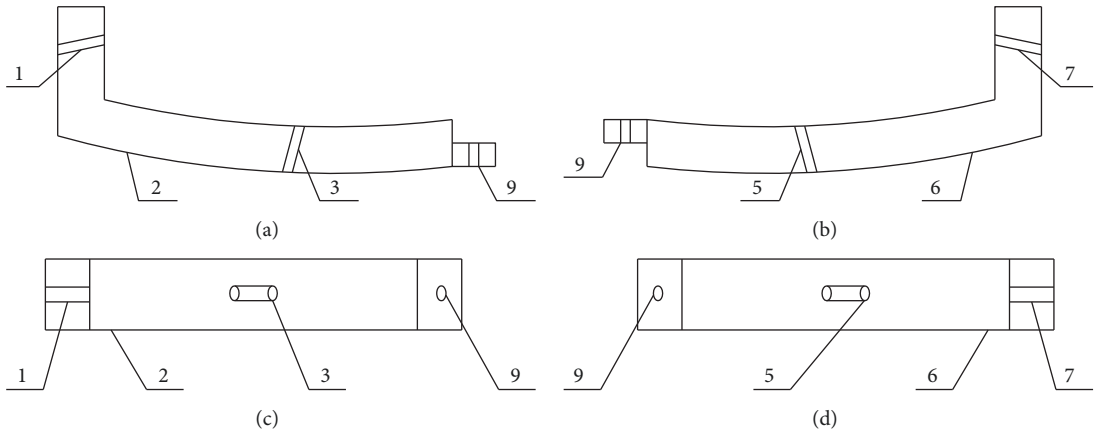

Figure 1: The schematic diagram of concrete inverted arches.

widths of roadway, filling body, and limit equilibrium zone of coal side. In Sun et al. study [17], in order to research mechanism and controlling method of strong floor heave in deep soft rock roadway, with the floor heave of southern main roadway in Handan MIG Tao'er coal mine expansion area as the engineering background, the characteristics and influence factors of strong floor heave in south main roadway were analyzed and the treatment scheme of cable beam and floor grouting was put forward. These measures can properly improve the stress state of the surrounding rock, strengthen the floor, and further restrain the floor heave. However, the ignorance of the reinforcement of the sidewalls, especially the destruction of the bottom and sidewalls, will cause floor heave and failure, because the component of the reinforced floor loses a concentration point in the sidewalls with high stresses [18, 19]. The cast-in-place concrete antiarch in the ground can reinforce the roadway floor and bottom corners and inhibit the floor heave. However, without bolts installed on the arch, this support may fail to control the roadway floor heave. In the present paper, we proposed a composite structure (a semiclosed structure) to strengthen the floor and the bottom sidewalls. Then, according to the relevant assumptions on the beam and mechanic theory of plate, we established a mechanical model for the composite structure to analyze the mechanism of floor heave. In addition, we established the stability equations of the bolt and concrete antiarch. Based on the specific conditions of the #1 roadway in the S6 mining area of the Changcun mine, the proposed support structure was installed. Moreover, we analyzed the stability and verified the feasibility of this composite system, by studying stability condition equations and conducting numerical simulations.

2. The Design of the Composite Structure

Two semicurved concrete structures with bolt holes were prefabricated (Figure 1). The length of the structure, with the section size of 250 × 250 mm, was determined by the width of the roadway. After the transportation to the underground working face, they were installed in a ditch on the floor and the two bottom sidewalls of the roadway. Bolts and plates, connecting the two arch shaped components, formed an inverted arch structure (Figure 2). Then, bolt holes and sidewall holes were extended with a rebar (22 mm in diameter). Finally, the void space was filled with concrete to connect the concrete antiarch components, the floor, and the sidewalls. In the floor deformation process, the composite structure and the anchoring force of the bolt can contribute to controlling the floor heave. The bearing force of the arch included the bolt force and the reactive force of the surrounding rock on the arch feet. The bearing force can strengthen the arch feet and effectively resist the floor pressure. The composite structure strengthened the structure and the surrounding rock and fully utilized the bearing capacity of the component and the surrounding rock. Thus, this system may properly restrain floor heave.

Figure 1 shows the prefabricated concrete antiarch components 2 and 6. In Figures 1(a) and 1(c), the inclination angle and diameter of bolt hole 1 were 12° and 32 mm, respectively. The inclination angle and diameter of bolt hole 3 were 70° and 32 mm, and the diameter of the connecting bolt hole 9 was 24 mm. In Figures 1(b) and 1(d), the inclination angle of bolt hole 5 with a diameter of 32 mm was 110°. The inclination angle and diameter of bore hole 7 were 168° and 32 mm.

In the implementation process (Figure 2), first, a ditch was dug for the concrete antiarch structure in the roadway floor and the bottom sidewalls. Concrete antiarch structures 2 and 6 were connected by bolt 4 (M22) and the cushion blocks 8. Then, the bottom bolts 10 were installed in the extended bore holes 3 and 5. Subsequently, bottom corner anchors 11 were installed in the extended bolt holes 1 and 7. Finally, cast-in-place concrete filled the gap between the composite structure and the ditch surfaces.

3. The Establishment and Mechanical Analysis of the Mechanical Model Characterized by Bolts and Concrete Antiarches

3.1. The Establishment of the Mechanical Model for the Floor Heave Control. Based on the theory of mechanics [20, 21], we studied the surrounding rock at the shallow roadway. Figure 3 shows the mechanical model for the floor heave control, using bolts and concrete bolted antiarches.

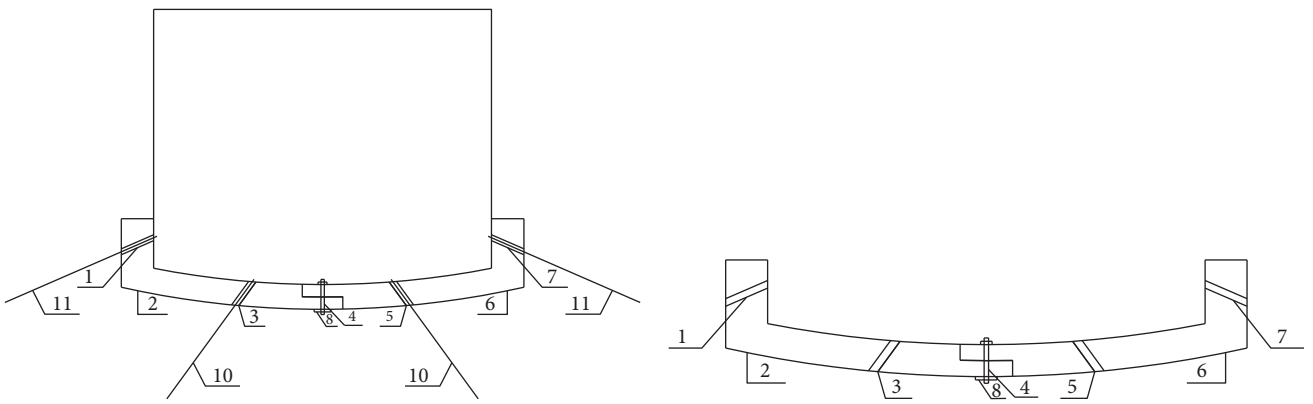

Figure 2: The schematic diagram of component installation. 1, 3, 5, and 7 bolt hole; 2, 6 split arch structure of precast concrete; 4 bolt; 8 cushion block; 9 bolt connection hole; 10 floor bolt; 11 bottom corner bolt.

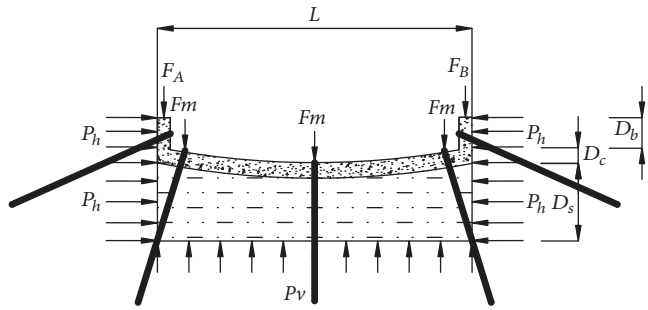

Figure 3: The mechanical model using a bolted antiarch structure.

In this model, P_h is the horizontal stress, acting on the concrete antiarches, and the anchorage bodies on the floor, MPa; P_v is the corresponding vertical stresses, MPa; F_m is the support force, formed by the floor bolts acting on the upper surface of the concrete antiarches, MPa; D_b is the height of the arch angle, m; D_c is the thickness of the concrete layer, m; D_s is the thickness of the surrounding rock on the floor, m; L is the span of the roadway, m.

3.2. Mechanical Analysis of the Floor Heave. The shallow surrounding rock in the anchored area and the concrete antiarch structure form a horizontal composite beam, subjected to vertical and horizontal stresses. When floor heave occurs, along the longitudinal direction of the roadway, the analysis of the horizontal beam with a length of b shows that [22]

$$\frac{1}{\rho} = \frac{M}{EJ} \tag{1}$$

where $1/\rho$ is the curvature of the deformed beam axis, m^{-1}; M is the bending moment of the horizontal beam, kN·m; E is the elastic modulus of the horizontal beam, GPa; J is the inertia moment of the cross section of the horizontal beam, $J = bD^3/12$, m^4; and D is the thickness of the horizontal beam, m, $D = D_c + D_s$.

When flexural deformation occurs, the same deformation curvature of the strata is

$$\frac{1}{\rho} = \frac{M_c}{E_c J_c} = \frac{M_s}{E_s J_s} \tag{2}$$

where $E = E_c(D_c/D) + E_s(D_s/D)$, $D = D_c + D_s$, and $M_c + M_s = M$.

Thus, the moment equation of every rock stratum is

$$M_c = \frac{M \cdot E_c J_c}{E_c J_c + E_c J_c}$$
$$M_q = \frac{M \cdot E_s J_s}{E_s J_s + E_s J_s} \tag{3}$$

If Q_c and Q_s are equal to $E_c J_c/(E_c J_c + E_c J_c)$ and $E_s J_s/(E_s J_s + E_s J_s)$, respectively, then, M_c, M_s are $Q_c M$ and $Q_s M$.

(1) *Supported by n bolts*

Based on the material mechanics, the moment equations of the horizontal beam, supported by n bolts, are

$$M(x) = \begin{cases} -\dfrac{P_v L}{2}x + \dfrac{P_v x^2}{2} - P_h D w + \dfrac{F_m\left(nL - \sum_{i=1}^{n}(n-i+1)\,a_i\right)}{L}x - \dfrac{P_h D_b^2}{2} & (0 \le x \le a_1) \\ -\dfrac{P_v L}{2}x + \dfrac{P_v x^2}{2} - P_h D w + \left[\dfrac{F_m\left((n-1)\,L - \sum_{i=1}^{n}(n-i+1)\,a_i\right)}{L}x + F_m a_1\right] - \dfrac{P_h D_b^2}{2} & (a_1 \le x \le a_2) \\ \cdots & \\ -\dfrac{P_v L}{2}x + \dfrac{P_v x^2}{2} - P_h D w + \left[\dfrac{F_m\left((n-j)\,L - \sum_{i=1}^{n}((n-i+1)\,a_i)\right)}{L}x + F_m\sum_{i=1}^{j}((j-i+1)\,a_i)\right] - \dfrac{P_h D_b^2}{2} & (a_j \le x \le a_{j+1}) \\ -\dfrac{P_v L}{2}x + \dfrac{P_v x^2}{2} - P_h D w + \left[-\dfrac{F_m\left(\sum_{i=1}^{n}(n-i+1)\,a_i\right)}{L}x + F_m\sum_{i=1}^{n}((n-i+1)\,a_i)\right] - \dfrac{P_h D_b^2}{2} & (a_n \le x \le L) \end{cases} \tag{4}$$

where j represents the Jth section, determined by n root bolts ($j = 1, 2, 3, 4 \ldots n$).

The general solution of ordinary differential equation with a polynomial order of 2 is

$$w_j = A_j \cos(hx) + B_j \sin(hx) + \frac{P_v L x^2 + \left[2F_m\left((n-j)\,L - \sum_{i=1}^{n}((n-i+1)\,a_i)\right) - P_v L^2\right]x + 2LF_m\sum_{i=1}^{j}((j-i+1)\,a_i) - {P_h}^2 D D_b^2 - 2LP_v/h^2}{2P_h DL} \tag{5}$$

where h^2 is equal to $P_h D/EJ$, and j=1,2,3$\cdots n$. Then, the moment equation of the Jth section J is

$$M_j(x) = -\frac{P_v L}{2}x + \frac{P_v x^2}{2} - P_h D w + \left[\frac{F_m\left((n-j)\,L - \sum_{i=1}^{n}((n-i+1)\,a_i)\right)}{L}x + F_m\sum_{i=1}^{j}((j-i+1)\,a_i)\right] - {P_h}^2 D D_b^2 \tag{6}$$

Namely,

$$M_j(x) = -P_h D\left[A_j \cos(hx) + B_j \sin(hx) - \frac{P_v}{P_h D h^2}\right] \tag{7}$$

The corresponding shear equation is

$$Fs_j(x) = P_h D h\left[A_j \sin(hx) - B_j \cos(hx)\right] \tag{8}$$

(2) Supported by n bolts with the same spacing
The deflection equation of the horizontal beam is

$$w_j = A_j \cos(hx) + B_j \sin(hx) + \frac{P_v}{2P_h D}x^2 + \left(\frac{F_m n - P_v L}{2P_h D} - \frac{jF_m}{P_h D}\right)x + \frac{j(j+1)\,F_m L}{2(n+1)\,P_h D} - \frac{P_v}{P_h D h^2} - \frac{P_h D_b^2}{2} \quad a_j \le x \le a_{j+1} \tag{9}$$

According to the symmetry of the beam, the boundary conditions of the deflection, the moment, and the shear stress of the horizontal beam are

$$\begin{aligned} w_j(x)\big|_{x=(j/(n+1))L} &= w_{j-1}(x)\big|_{x=(j/(n+1))L} \\ w_{n-j}(x)\big|_{x=((n-j)/(n+1))L} &= w_{n-j+1}(x)\big|_{x=((n-j)/(n+1))L} \\ M_j(x)\big|_{x=(j/(n+1))L} &= M_{j-1}(x)\big|_{x=(j/(n+1))L} \\ M_{n-j}(x)\big|_{x=((n-j)/(n+1))L} &= M_{n-j+1}(x)\big|_{x=((n-j)/(n+1))L} \\ Fs_j(x)\big|_{x=(j/(n+1))L} &= Fs_{j-1}(x)\big|_{x=(j/(n+1))L} + F_m \end{aligned} \tag{10}$$

Simultaneously, at both ends of the horizontal beam, the boundary conditions are

$$\begin{aligned} M_1(x)\big|_{x=0} &= -\frac{P_h D_b^2}{2}, \\ M_n(x)\big|_{x=L} &= -\frac{P_h D_b^2}{2} \end{aligned} \tag{11}$$

Shear stresses are

$$Fs_j(x)\big|_{x=(j/(n+1))L} = Fs_{j-1}(x)\big|_{x=(j/(n+1))L} + F_m, \tag{12}$$

List the equations as follows:

$$\begin{aligned} Fs_j\left(\frac{j}{n+1}L\right) &= P_h Dh\left[A_j \sin\left(\frac{j}{n+1}Lh\right)\right. \\ &\quad \left. - B_j \cos\left(\frac{j}{n+1}Lh\right)\right] \\ Fs_{j-1}\left(\frac{j}{n+1}L\right) &= P_h Dh\left[A_{j-1} \sin\left(\frac{j}{n+1}Lh\right)\right. \\ &\quad \left. - B_{j-1} \cos\left(\frac{j}{n+1}Lh\right)\right] \end{aligned} \tag{13}$$

Then there are

$$\begin{aligned} &A_j \sin\left(\frac{j}{n+1}Lh\right) - B_j \cos\left(\frac{j}{n+1}Lh\right) \\ &\quad = A_{j-1} \sin\left(\frac{j}{n+1}Lh\right) - B_{j-1} \cos\left(\frac{j}{n+1}Lh\right) \\ &\quad + \frac{F_m}{P_h Dh} \end{aligned} \tag{14}$$

At the same time, at the point of the anchorage position, there are

$$\begin{aligned} M_j\left(\frac{j}{n+1}L\right) &= -P_h D\left[A_j \cos\left(\frac{j}{n+1}Lh\right)\right. \\ &\quad \left. + B_j \sin\left(\frac{j}{n+1}Lh\right) - \frac{P_v}{P_h Dh^2}\right] \\ M_{j-1}\left(\frac{j}{n+1}L\right) &= -P_h D\left[A_{j-1} \cos\left(\frac{j}{n+1}Lh\right)\right. \\ &\quad \left. + B_{j-1} \sin\left(\frac{j}{n+1}Lh\right) - \frac{P_v}{P_h Dh^2}\right] \end{aligned} \tag{15}$$

Then there are

$$\begin{aligned} &A_j \cos\left(\frac{j}{n+1}Lh\right) + B_j \sin\left(\frac{j}{n+1}Lh\right) \\ &\quad = A_{j-1} \cos\left(\frac{j}{n+1}Lh\right) + B_{j-1} \sin\left(\frac{j}{n+1}Lh\right) \end{aligned} \tag{16}$$

Combined formula (14) and formula (16) can be solved:

$$\begin{aligned} A_j &= A_{j-1} + \frac{F_m}{P_h Dh} \sin\left(\frac{j}{n+1}Lh\right) \\ B_j &= B_{j-1} - \frac{F_m}{P_h Dh} \cos\left(\frac{j}{n+1}Lh\right) \end{aligned} \tag{17}$$

According to the boundary conditions, we can obtain

$$\begin{aligned} A_j &= A_1 + \frac{F_m}{P_h Dh} \sum_{t=1}^{j} \sin\left(\frac{t}{n+1}Lh\right) \\ B_j &= B_1 - \frac{F_m}{P_h Dh} \sum_{t=1}^{j} \cos\left(\frac{t}{n+1}Lh\right) \end{aligned} \tag{18}$$

The boundary conditions at the ends of the horizontal beam are $M_1(x)|_{x=0} = -P_h D_b^2/2$, $M_n(x)|_{x=L} = -P_h D_b^2/2$; therefore, we can obtain that

$$\begin{aligned} M_1(0) &= -P_h D\left[A_1 \cos(0) + B_1 \sin(0) - \frac{P_v}{P_h Dh^2}\right] \\ &= \frac{P_h D_b^2}{2} \end{aligned} \tag{19}$$

The above analysis yields

$$\begin{aligned} A_j &= \left(\frac{P_v}{P_h Dh^2} + \frac{D_b^2}{2D}\right) + \frac{F_m}{P_h Dh} \sum_{t=1}^{j} \sin\left(\frac{t}{n+1}Lh\right) \\ B_j &= \left(\frac{P_v}{P_h Dh^2} + \frac{D_b^2}{2D}\right)\left(\frac{1}{\sin(hL)} - \cot(hL)\right) \\ &\quad + \frac{F_m}{P_h Dh}\left(\sum_{t=1}^{n} \cos\left(\frac{t}{n+1}Lh\right)\right. \\ &\quad \left. - \cot(hL) \sum_{t=1}^{n} \sin\left(\frac{t}{n+1}Lh\right)\right) - \frac{F_m}{P_h Dh} \\ &\quad \cdot \sum_{t=1}^{j} \cos\left(\frac{t}{n+1}Lh\right) \end{aligned} \tag{20}$$

The same spacing between bolts and symmetry of the horizontal beam result in that the maximum deflection and moment will occur at the middle position of the horizontal beam. Therefore, according to the above analysis, we can obtain the mechanical equation coefficients at the middle position of the horizontal beam, the maximum values of the deflection, the moment, the shear stress and the normal stress, and the shear stress equation of the horizontal beam.

① when n is an odd number

The mechanical equation coefficients, at the middle position of the horizontal beam, are

$$\begin{aligned} A_{(n+1)/2} &= \left(\frac{P_v}{P_h Dh^2} + \frac{D_b^2}{2D}\right) + \frac{F_m}{P_h Dh} \\ &\quad \cdot \sum_{t=1}^{(n+1)/2} \sin\left(\frac{t}{n+1}Lh\right) \\ B_{(n+1)/2} &= \left(\frac{P_v}{P_h Dh^2} + \frac{D_b^2}{2D}\right)\left(\frac{1}{\sin(hL)} - \cot(hL)\right) \\ &\quad + \frac{F_m}{P_h Dh}\left(\sum_{t=1}^{n} \cos\left(\frac{t}{n+1}Lh\right)\right. \\ &\quad \left. - \cot(hL) \sum_{t=1}^{n} \sin\left(\frac{t}{n+1}Lh\right)\right) - \frac{F_m}{P_h Dh} \\ &\quad \cdot \sum_{t=1}^{(n+1)/2} \cos\left(\frac{t}{n+1}Lh\right) \end{aligned} \tag{21}$$

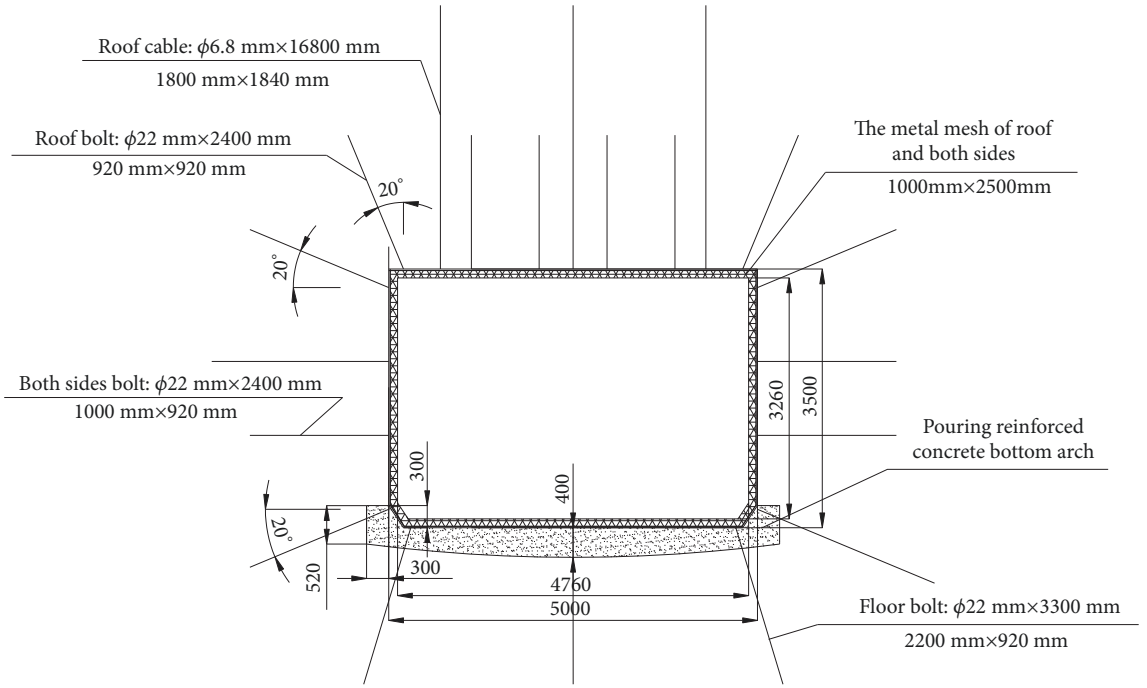

Figure 4: The support section of the composite system.

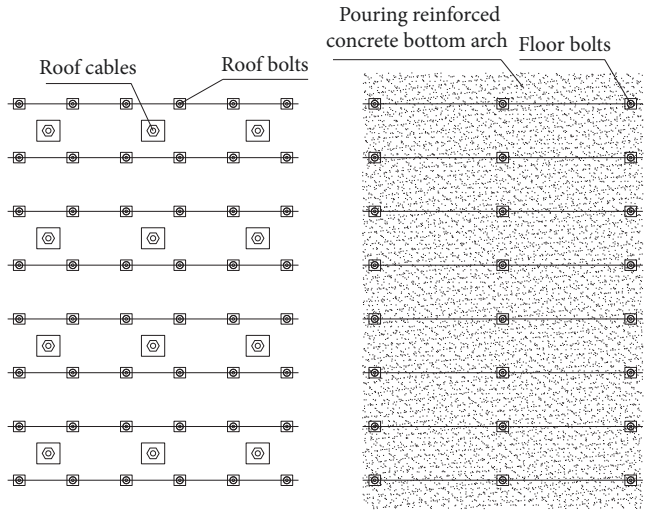

Figure 5: The support layout of the roof and the floor.

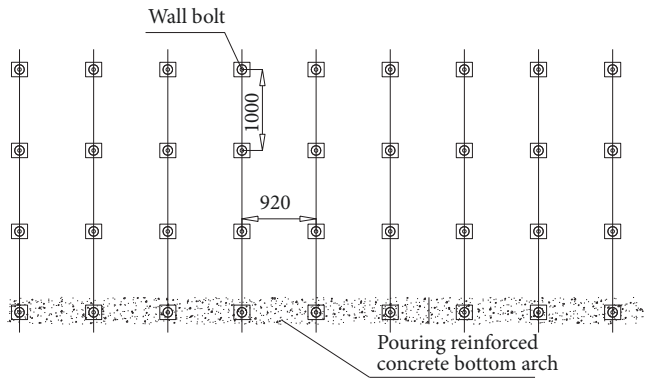

Figure 6: The support layout of the sidewalls.

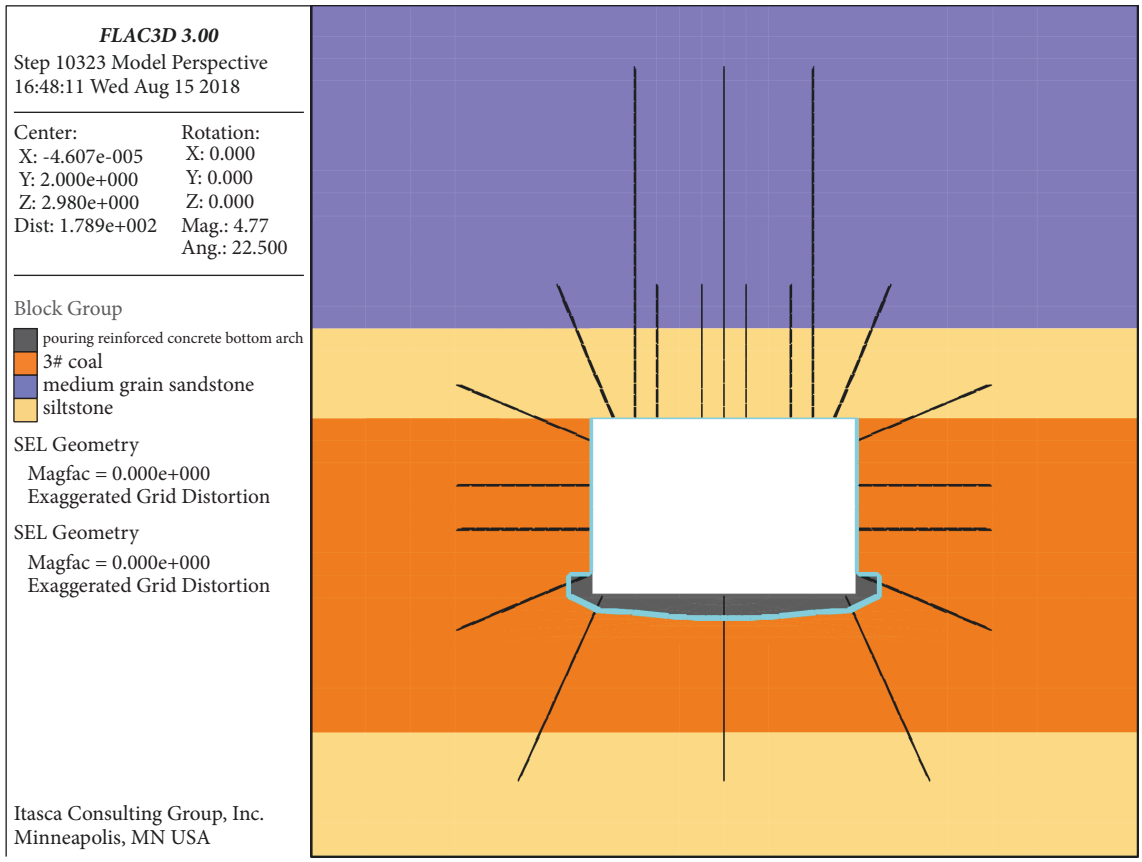

Figure 7: The layout of the support system and roadway strata.

The maximum values of the deflection, the moment, the shear force and the normal stress, and the shear stress equation of the composite floor horizontal beam are

$$w_{\max} = w_{(n+1)/2}\left(\frac{L}{2}\right) = A_{(n+1)/2}\cos\left(\frac{Lh}{2}\right) + B_{(n+1)/2} \cdot \sin\left(\frac{Lh}{2}\right) + \frac{F_m(n+1) - P_v L}{8P_h D} - \frac{P_v}{P_h D h^2} - \frac{P_h D_b^2}{2}$$

$$M_{\max} = M_{(n+1)/2}\left(\frac{L}{2}\right) = -P_h D\left[A_{(n+1)/2}\cos\left(\frac{Lh}{2}\right) + B_{(n+1)/2}\sin\left(\frac{Lh}{2}\right) - \frac{P_v}{P_h D h^2}\right]$$

$$Fs_{\max} = Fs_1(0) = P_h Dh\left[A_1\sin(0) - B_1\cos(0)\right] \quad (22)$$

$$\sigma_{\max} = \sigma_{(n+1)/2}\left(\frac{L}{2}\right) = P_h D\left[A_{(n+1)/2}\cos\left(\frac{Lh}{2}\right) + B_{(n+1)/2}\sin\left(\frac{Lh}{2}\right) - \frac{P_v}{P_h D h^2}\right]\frac{y}{J} - P_h$$

$$\tau_{\max} = \tau_1(0) = -\frac{P_h Dh}{2J}\left[A_1\sin(0) - B_1\cos(0)\right]\left(\frac{D^2}{4} - y^2\right)$$

② when n is an even number

The mechanical equation coefficients, at the middle position of the horizontal beam, are

$$A_{n/2} = \left(\frac{P_v}{P_h D h^2} + \frac{D_b^2}{2D}\right) + \frac{F_m}{P_h Dh}\sum_{t=1}^{n/2}\sin\left(\frac{t}{n+1}Lh\right)$$

$$B_{n/2} = \left(\frac{P_v}{P_h D h^2} + \frac{D_b^2}{2D}\right)\left(\frac{1}{\sin(hL)} - \cot(hL)\right) + \frac{F_m}{P_h Dh}\left(\sum_{t=1}^{n}\cos\left(\frac{t}{n+1}Lh\right) - \cot(hL)\sum_{t=1}^{n}\sin\left(\frac{t}{n+1}Lh\right)\right) - \frac{F_m}{P_h Dh} \cdot \sum_{t=1}^{n/2}\cos\left(\frac{t}{n+1}Lh\right) \quad (23)$$

The maximum values of the deflection, the moment, the shear force and the normal stress, and the shear stress equation of the composite floor horizontal beam are

$$w_{\max} = w_{n/2}\left(\frac{L}{2}\right) = A_{n/2}\cos\left(\frac{Lh}{2}\right) + B_{n/2}\sin\left(\frac{Lh}{2}\right) + \frac{F_m n(n+3) - P_v L}{8(n+1)P_h D} - \frac{P_v}{P_h D h^2} - \frac{P_h D_b^2}{2}$$

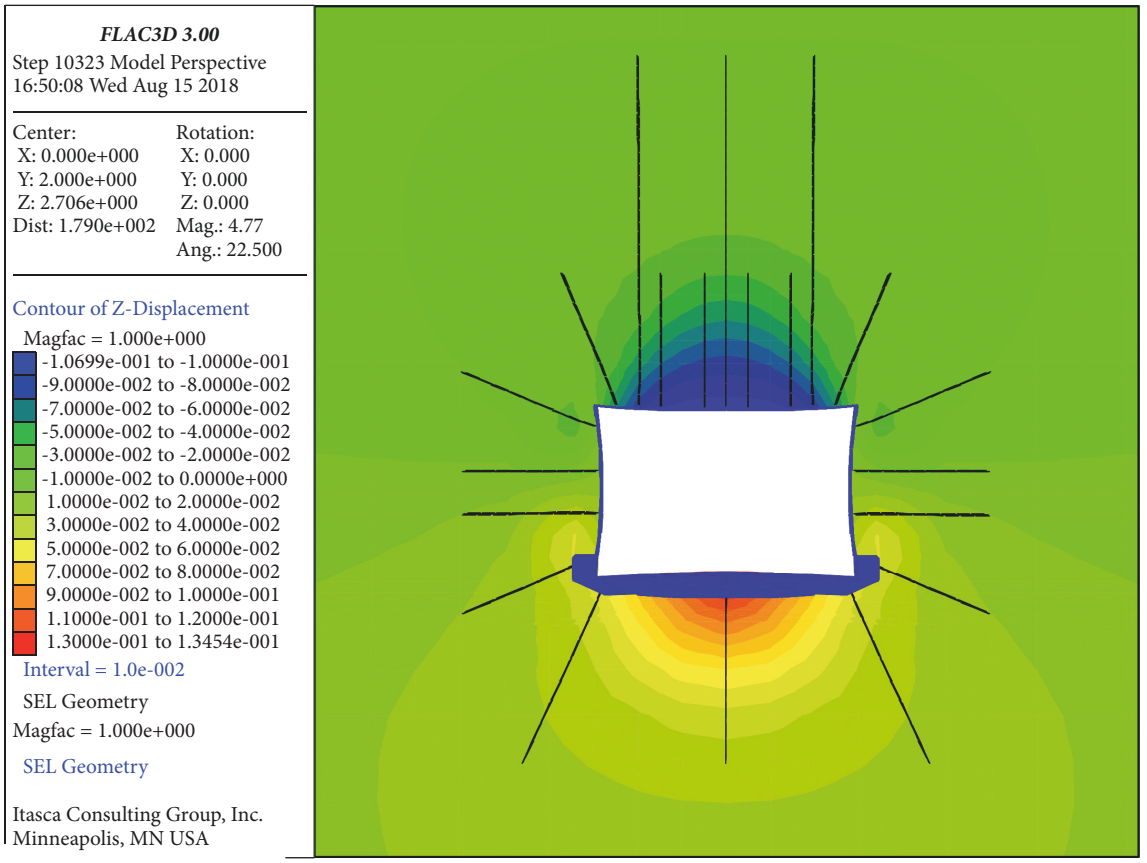

Figure 8: The vertical displacement of the roadway after installing the composite structure.

$$
\begin{aligned}
M_{\max} &= M_{n/2}\left(\frac{L}{2}\right) = -P_h D\left[A_{n/2}\cos\left(\frac{Lh}{2}\right)\right.\\
&\quad \left. + B_{n/2}\sin\left(\frac{Lh}{2}\right) - \frac{P_v}{P_h D h^2}\right]\\
Fs_{\max} &= Fs_1(0) = P_h D h\left[A_1\sin(0) - B_1\cos(0)\right]\\
\sigma_{\max} &= \sigma_{n/2}\left(\frac{L}{2}\right) = P_h D\left[A_{n/2}\cos\left(\frac{Lh}{2}\right)\right.\\
&\quad \left. + B_{n/2}\sin\left(\frac{Lh}{2}\right) - \frac{P_v}{P_h D h^2}\right]\frac{y}{J} - P_h\\
\tau_{\max} &= \tau_1(0) = -\frac{P_h D h}{2J}\left[A_1\sin(0) - B_1\cos(0)\right]\left(\frac{D^2}{4}\right.\\
&\quad \left. - y^2\right)
\end{aligned}
\tag{24}
$$

(3) The deformation equations of the concrete antiarches are

$$
\begin{aligned}
w_c &= w\\
M_c &= Q_c M\\
Fs_c &= Q_c Fs\\
\sigma_c &= Q_c \sigma\\
\tau_c &= Q_c \tau\\
&\quad \left(-\frac{D}{2} + D_s \le y \le \frac{D}{2}\right)
\end{aligned}
\tag{25}
$$

$$
\begin{aligned}
w_s &= w\\
M_s &= Q_s M\\
Fs_s &= Q_s Fs\\
\sigma_s &= Q_s \sigma\\
\tau_s &= Q_s \tau\\
&\quad \left(-\frac{D}{2} \le y < -\frac{D}{2} + D_s\right)
\end{aligned}
\tag{26}
$$

3.3. Stability Criterion of the Composite Structure. According to the above mechanical analyses, to ensure the stability of the composite structure subjected to underground stresses, the stress conditions of the structure material should satisfy

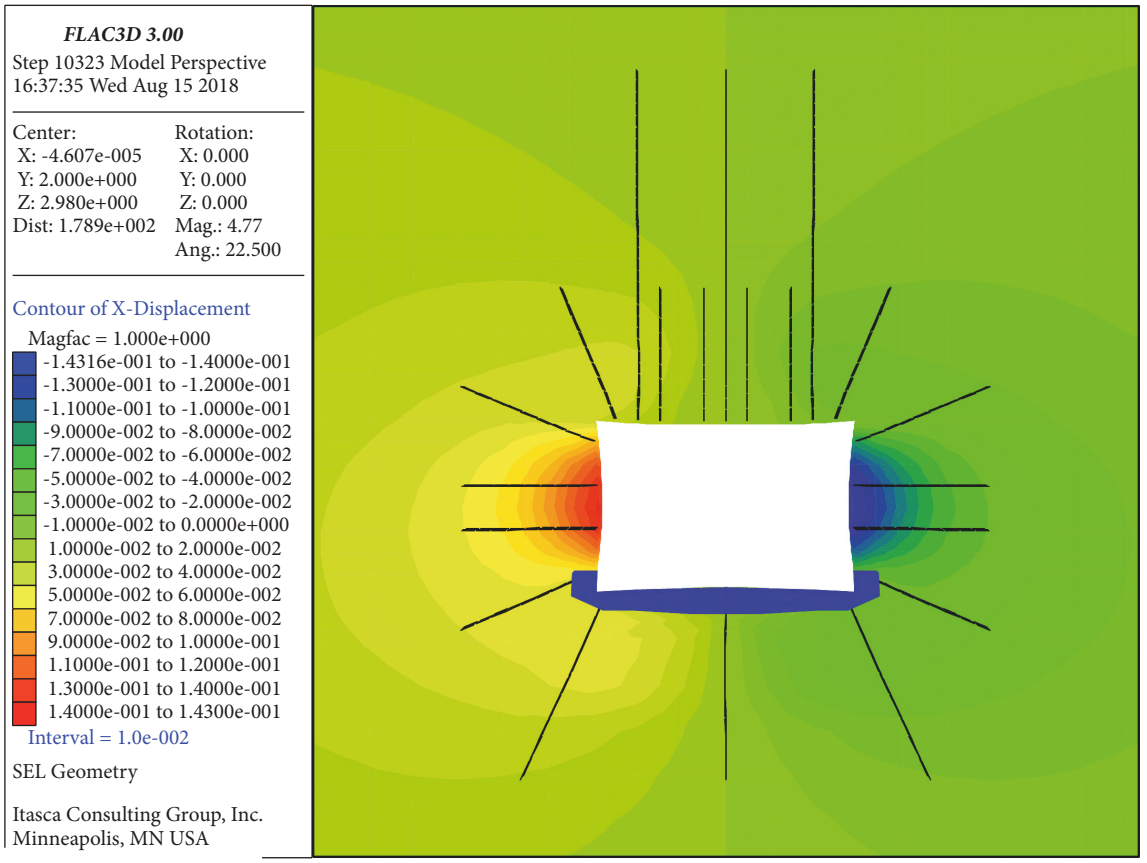

Figure 9: The level displacement of the roadway after installing the composite structure.

$$\begin{aligned} &\sigma_{t\max} \le [\sigma_t]; \\ &|\tau_{\max}| \le |\sigma_{\max}| \tan(\varphi) + \sigma_c \end{aligned} \tag{27}$$

Based on the mechanical equation of the composite structure, the normal (tensile) stress of the structure mainly acts on the upper boundary at the middle part, whereas the maximum shear stress is located on the neutral surfaces near the structure ends. Therefore, two destructive forms may occur.

(1) When the maximum normal stress of the structure, $\sigma_{t\max}$, is higher than $[\sigma_t]$, tensile failure at the upper surface of the middle point first occurs. The composite structure fails at the middle of the floor because of the tensile bending.

(2) When the shear stress, $|\tau_{\max}|$, is higher than $|\sigma_{\max}| \tan(\varphi) + \sigma_c$, shear failure first occurs at the middle parts of the end because the shear stress exceeds the shear limit on the neutral surfaces.

Therefore, the stability equations of the composite structure are as follows:

① when n is an odd number

$$\begin{aligned} &\left|\left(\frac{E_cJ_c}{E_sJ_s + E_cJ_c}\right)\left[A_{(n+1)/2}\cos\left(\frac{Lh}{2}\right) + B_{(n+1)/2}\sin\left(\frac{Lh}{2}\right) - \frac{P_v}{P_hDh^2}\right]\frac{P_hD^2}{4J} - P_h\right| \\ &\le [\sigma_t]_c\left|-\frac{P_hDh}{2J}\left(\frac{E_cJ_c}{E_sJ_s + E_cJ_c}\right)[A_1\sin(0) - B_1\cos(0)]\left(\frac{D^2}{4}\right)\right| \le \left|-\left(\frac{E_cJ_c}{E_sJ_s + E_cJ_c}\right)\right. \\ &\cdot\left[A_{(n+1)/2}\cos\left(\frac{Lh}{2}\right) + B_{(n+1)/2}\sin\left(\frac{Lh}{2}\right) - \frac{P_v}{P_hDh^2}\right]\frac{P_hD^2}{4J} - P_h\left|\tan(\varphi_c) + [\sigma_c]_c\right. \end{aligned} \tag{28}$$

② when n is an even number

$$\begin{aligned} &\left|\left(\frac{E_cJ_c}{E_sJ_s + E_cJ_c}\right)\cdot\left[A_{n/2}\cos\left(\frac{Lh}{2}\right) + B_{n/2}\sin\left(\frac{Lh}{2}\right) - \frac{P_v}{P_hDh^2}\right]\cdot\frac{P_hD^2}{4J} - P_h\right| \le [\sigma_t]_c\left|-\frac{P_hDh}{2J}\left(\frac{E_cJ_c}{E_sJ_s + E_cJ_c}\right)\right. \\ &\cdot[A_1\sin(0) - B_1\cos(0)]\left(\frac{D^2}{4}\right)\Bigg| \end{aligned}$$

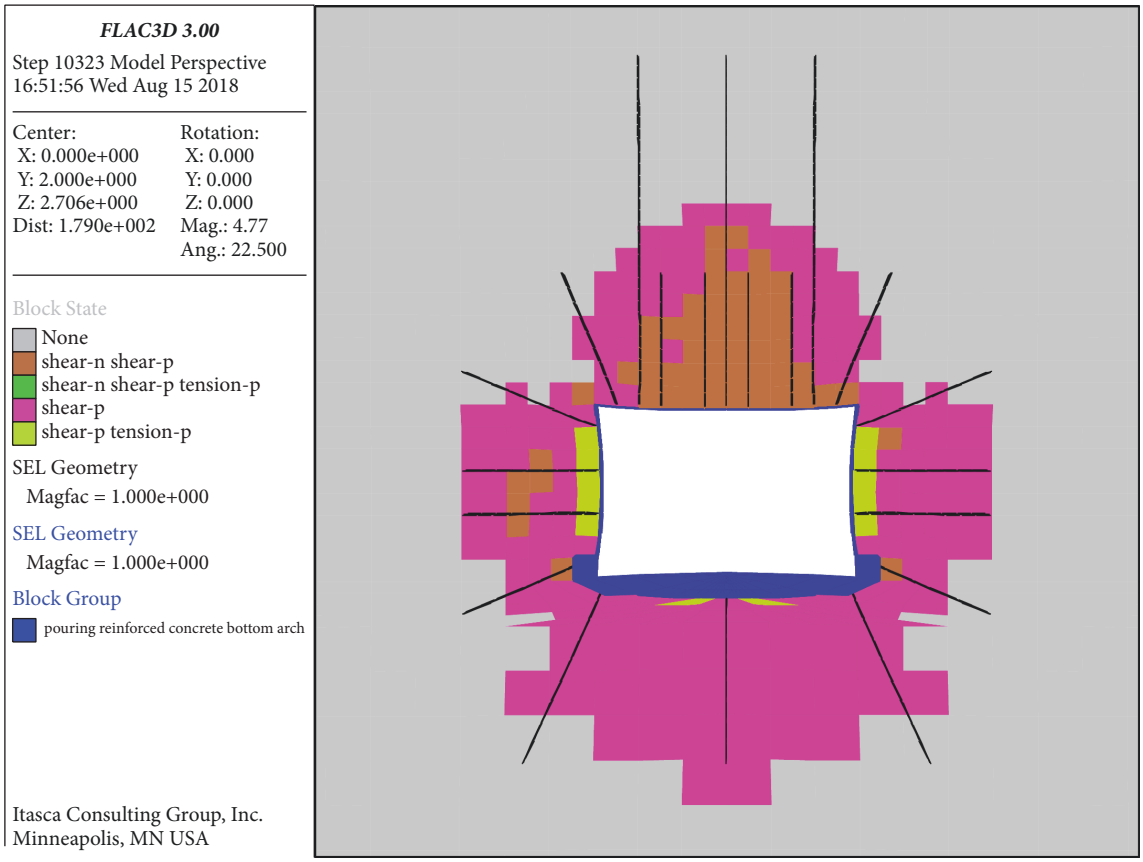

Figure 10: The plastic zones in surrounding rocks.

$$\leq \left| -\left(\frac{E_c J_c}{E_s J_s + E_c J_c}\right) \cdot \left[A_1 \cos(0) + B_1 \sin(0) - \frac{P_v}{P_h D h^2}\right] \frac{P_h D^2}{4J} - P_h \right| \cdot \tan(\varphi_c) + [\sigma_c]_c \tag{29}$$

4. The Support Design for the Floor Heave Control at #1 Roadway in S6 Mining Area of Changcun Mine

4.1. The Support Scheme Design of Floor Heave Control. With the practical conditions at the #1 roadway in the S6 mining area of Changcun mine, we proposed a support system to control the floor heave (Figure 4). Figures 5 and 6 show the corresponding layout and parameters.

4.2. The Stability the Composite Structure. According to the geological data and design parameters of the roadway, the elastic modulus of the shallow surrounding rock E was 0.55 GPa [23, 24]. In addition, the width of the rectangular roadway was 5 m. However, considering the damage zone in the surrounding rock, the span of the floor was $L = 9$ m. Moreover, the C20 concrete with the elastic modulus, tensile strength, compressive strength, cohesion, and frictional angle of 25.5 GPa 1.1 MPa, 9.6 MPa, 2.0, and 45°, respectively, was applied to fabricate the concrete arches [25]. Considering the construction infeasibility at the corner between the floor and the sidewalls, the elastic modulus of the concrete antiarch layer with a thickness of 0.3 m was $E_c = 10$ GPa [24, 26]. The arch height at the corner was $D_b = 0.12$ m. Furthermore, the roadway floor was supported by 3 root bolts with the length, yield strength, and preanchorage force of 3.3 m, 300 MPa, and 100 kN, respectively. The total value of the composite structure thickness and plastic damage depth, D, was 3 m.

According to the stress transformation laws from the polar coordinate system to the Cartesian coordinate system, the horizontal stresses of the left and right boundaries, P_h, were 6.13 MPa. In addition, the corresponding vertical stresses, P_v, were 7.67 MPa.

Equation (28) yields

$$\left| \left(\frac{E_c J_c}{E_s J_s + E_c J_c}\right) \left[A_{(n+1)/2} \cos\left(\frac{Lh}{2}\right) + B_{(n+1)/2} \sin\left(\frac{Lh}{2}\right) - \frac{P_v}{P_h D h^2}\right] \frac{P_h D^2}{4J} - P_h \right| = 5.12 \text{ MPa} \tag{30}$$

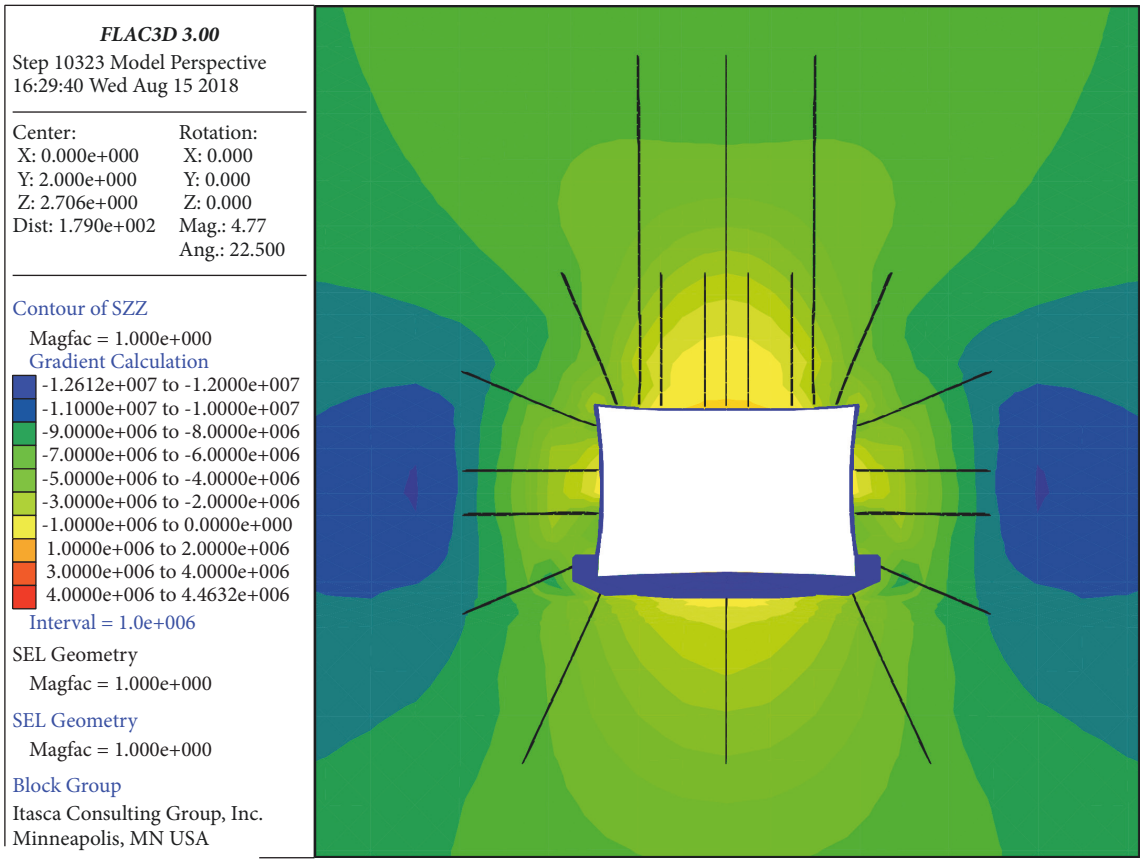

Figure 11: The vertical stress distribution.

The maximum tensile stress at the upper middle boundary of the composite structure was 9.6 MPa.

Thus, with the maximum compressive stress (5.3 MPa) at the bottom middle boundary, we can conclude that compressive failure will not occur.

$$\left|-\frac{P_h D h}{2J}\left(\frac{E_c J_c}{E_s J_s + E_c J_c}\right)\left[A_0 \sin(0) - B_0 \cos(0)\right] \cdot \left(\frac{D^2}{4}\right)\right| = 0.14\ \text{MPa} \tag{31}$$

The maximum shear stress on the neutral surfaces was

$$\left|-\left(\frac{E_c J_c}{E_s J_s + E_c J_c}\right)\left[A_{(n+1)/2} \cos\left(\frac{Lh}{2}\right) + B_{(n+1)/2} \sin\left(\frac{Lh}{2}\right) - \frac{P_v}{P_h D h^2}\right]\frac{P_h D^2}{4J} - P_h\right| \tan(\varphi_c) + [\sigma_c]_c = 14.76\ \text{MPa} = 14.76\ \text{MPa} \tag{32}$$

The calculated shear stress was much lower than the shear strength; thus, shear failure will not occur.

According to the above mechanical analysis, we conclude that the composite structure with a calculated deformation of 106.7 mm is stable and the parameters are reasonable.

4.3. Numerical Simulation

4.3.1. Stability Analysis of the Support Structures. Figure 7 shows the layout of the support system and the roadway strata. The roof bolts and anchor cables were installed in the medium-grained sandstone and siltstone strata above the roof. In addition, the sidewall bolts were installed in the coal seam because of the arrangement of the roadway. Due to the constraints of the surrounding rock, the bolts on the sidewalls were strengthened. Moreover, the bolts and concrete antiarches, providing sufficient support resistance, ensured the uniform stress distribution on the floor. Simultaneously, the slight effect of the floor deformation on the composite structure was favourable to the floor stability.

4.3.2. The Analysis of Deformation and Failure Characteristics of the Surrounding Rock. Figures 8 and 9 show the vertical and horizontal displacements. Clearly, because of the installation of the composite structure on the floor, the floor heave and the horizontal displacement on the sidewalls were only 135 mm and 286 mm, respectively. These small values show that the composite structure can successfully restrain the roadway deformation. "Concrete antiarches surrounding rock composite structure" overcome the defects that the supporting structure can not strengthen the surrounding rock of roadway bottom side in the current, while reinforcing the floor surrounding rock, the roadway both bottom sides

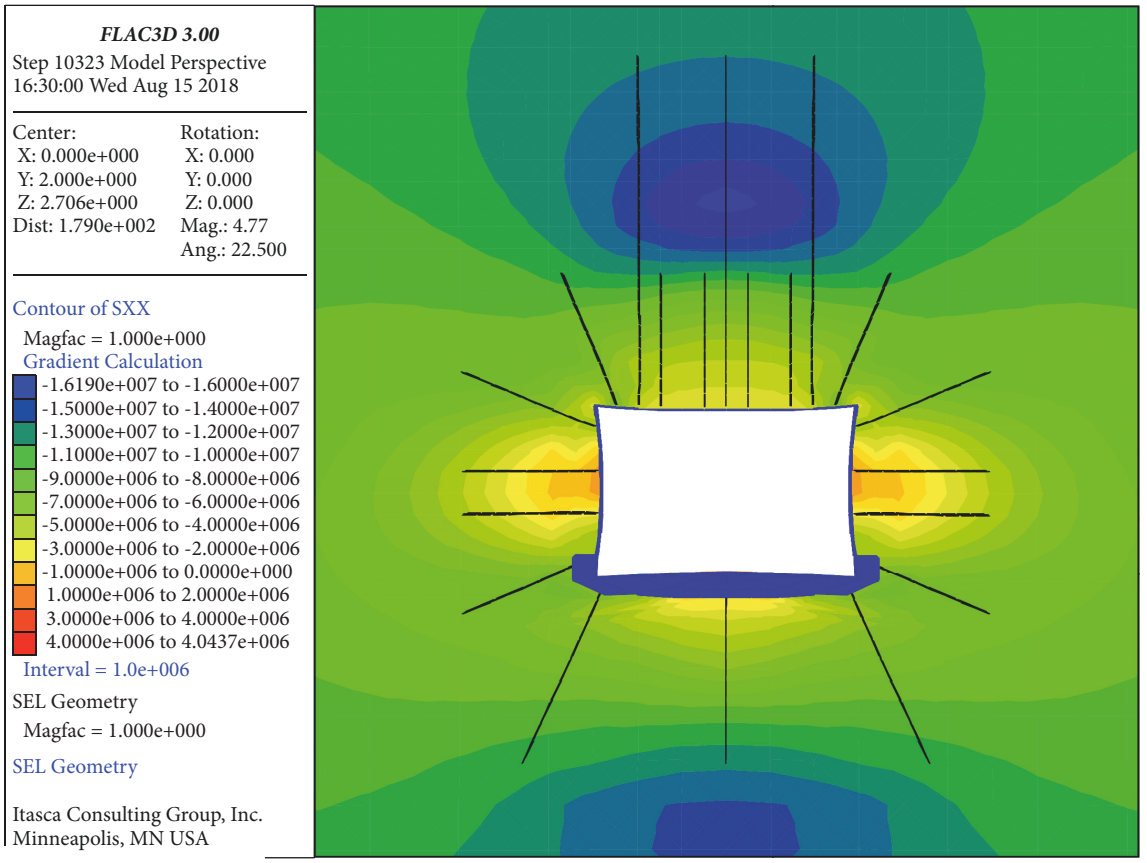

Figure 12: The horizontal stress distribution.

are also reinforced by the bottom angle bolt support, thereby forming a semiclosed structure, which solves the key problem that the floor failure caused by the bottom side failure and can not only effectively prevent floor heave but also enhance the stability of the roadway rib-to-rib.

Figure 10 shows the failure zone in the surrounding rock. The failure depths of the surrounding rock at the roof and floor corners were relatively small. In addition, the destruction depth on the roof partially exceeded the length of the bolt; however, the destructive depth failed to exceed the length of the cable. Moreover, the destruction depth of the sidewalls approximately exceeded the length of the short bolts. However, because the floor was strengthened by the composite structure, the bearing capacity of the surrounding rock was promoted. Therefore, with the support force of the long bolts, the support effect is satisfactory.

4.3.3. The Analysis of Stress Concentrations of the Surrounding Rock. Figures 11 and 12 indicate the vertical and horizontal stress distributions after the installation of the composite structure. The stress relaxation area formed in the shallow surrounding rock because of the failure in the surrounding rock. The horizontal stress concentration area of the surrounding rock, with a peak stress of 12.6 MPa, formed at the ends of the roof and floor bolts. The concentrated vertical stress, with the peak value of 46.2 MPa occurred at the end of both sidewall bolts. The stress concentrations of the surrounding rock mainly formed in the roof and the floor. This phenomenon indicates that the roof and floor are the key parts. This phenomenon is related to the stress environment of the roadway, because the higher horizontal stress frequently leads to stress concentrations in the roof and floor.

5. Conclusions

In the present article, first, we designed a composite structure, consisting of bolts and concrete antiarches. This structure may promote the bearing capacity of the structure and surrounding rock, prevent the deformation and destruction of the floor, and further control the floor heave. Then, based on relative assumptions, we established a mechanical model of the composite structure. We further analyzed the maximum deflection, moment, shear stress, and the maximum normal stress in the structure. In addition, we established the stability criterion for this model. Moreover, with the practical condition at the #1 roadway in S6 mining area of Changcun mine, we proposed a support system to control the roadway deformation. We verified the correctness of the design parameters of the system and obtained a predicted deformation of 106.7 mm. Furthermore, the numerical study shows that the proposed system successfully restrained the floor heave by 78.7%.

Data Availability

The (Figures 1–12) data used to support the findings of this study are included within the article. No other data were used to support this study.

Conflicts of Interest

The authors declare that there are no conflicts of interest regarding the publication of this paper.

Acknowledgments

This research is supported by the National Natural Science Foundation of China (nos. 51774131, 51274097, and 51434006), the CRSRI Open Research Program (CKWV2017508/KY), the Open Projects of State Key Laboratory of Coal Resources and Safe Mining, CUMT (no. SKLCRSM16KF12), High School Science research project of the Inner Mongolia Autonomous Region (NJZY16158), and Inner Mongolia University of Science and Technology and Innovation Fund Project (2015QDL01)

References

[1] X. Zhai, G. Huang, C. Chen, and R. Li, "Combined Supporting Technology with Bolt-Grouting and Floor Pressure-Relief for Deep Chamber: An Underground Coal Mine Case Study," *Energies*, vol. 11, no. 1, p. 67, 2018.

[2] X. Y. Zhang, T. Liu, G. Chen, and H. W. Liu, "Study of Floor Heave Mechanism in Deep Soft Rock Roadway," *Environment and Sustainable Development (APEESD)*, pp. 164–167, 2017.

[3] W. Zhang, Z. He, D. Zhang, D. Qi, and W. Zhang, "Surrounding rock deformation control of asymmetrical roadway in deep three-soft coal seam: a case study," *Journal of Geophysics and Engineering*, vol. 15, no. 5, pp. 1917–1928, 2018.

[4] Z. Zhou, C.-Q. Zhu, Q.-F. Li, and Y.-E. Shi, "The mechanism of mining roadway floor heave and its control measures," *Electronic Journal of Geotechnical Engineering*, vol. 20, no. 21, pp. 11467–11475, 2015.

[5] H. Li, F. Yu, Y. Ji, and H. Zhou, "Support controlling on shear type floor heave deformation in coal roadway," *Boletin Tecnico/Technical Bulletin*, vol. 55, no. 3, pp. 348–355, 2017.

[6] Y. Zhao, L. Zhang, W. Wang, W. Wan, and W. Ma, "Separation of Elastoviscoplastic Strains of Rock and a Nonlinear Creep Model," *International Journal of Geomechanics*, vol. 18, no. 1, p. 04017129, 2018.

[7] K. Perry, J. Bradley, K. Unrug, and M. Klimek, "Mitigation of floor heave in West Kentucky Coal Mine," *International Journal of Mining Science and Technology*, vol. 26, no. 3, pp. 521–525, 2016.

[8] H. Maleki, C. Stewart, R. Stone, J. Abshire, and J. Whyatt, "Analysis of sudden floor heave in deep western U.S. mines," in *Proceedings of the SME Annual Meeting and Exhibit and CMA's 111th National Western Mining Conference 2009*, pp. 54–62, February 2009.

[9] Y. Zhao, N. Liu, X. Zheng, and N. Zhang, "Mechanical model for controlling floor heave in deep roadways with U-shaped steel closed support," *International Journal of Mining Science and Technology*, vol. 25, no. 5, pp. 713–720, 2015.

[10] S.-Q. Yang, M. Chen, H.-W. Jing, K.-F. Chen, and B. Meng, "A case study on large deformation failure mechanism of deep soft rock roadway in Xin'An coal mine, China," *Engineering Geology*, vol. 217, pp. 89–101, 2017.

[11] H. S. Tu, S. H. Tu, C. Wang, D. Y. Hao, and D. F. Zhou, "Mechanical analysis of a vertical-wall, semicircular-arch roadway and a repair technique using double-shell support," *Environmental Earth Sciences*, vol. 77, no. 13, 2018.

[12] Y. Kang, Q. Liu, G. Gong, and H. Wang, "Application of a combined support system to the weak floor reinforcement in deep underground coal mine," *International Journal of Rock Mechanics and Mining Sciences*, vol. 71, pp. 143–150, 2014.

[13] G. Guo, H. Kang, D. Qian, F. Gao, and Y. Wang, "Mechanism for Controlling Floor Heave of Mining Roadways Using Reinforcing Roof and Sidewalls in Underground Coal Mine," *Sustainability* , vol. 10, no. 5, p. 1413, 2018.

[14] Z. Zhang and H. Shimada, "Numerical Study on the Effectiveness of Grouting Reinforcement on the Large Heaving Floor of the Deep Retained Goaf-Side Gateroad: A Case Study in China," *Energies*, vol. 11, no. 4, p. 1001, 2018.

[15] Y. Hou, S. Han, S. He, and X. Zhang, "Floor heave support measures of dongyi auxiliary transportation main roadway of liujia coal mine, China," *Electronic Journal of Geotechnical Engineering*, vol. 21, no. 23, pp. 7099–7111, 2016.

[16] X. Y. Liu and Y. F. Yu, "Calculation of Floor Deformation in Gob-Side Entry Retaining with Great-Depth and Large-Section," in *Proceedings of the 2016 International Conference on Applied Mechanics, Electronics and Mechatronics Engineering (Ameme 2016)*, pp. 162–167, 2016.

[17] L. H. Sun, B. S. Yang, C. D. Sun, X. Li, and Z. W. Wang, "Experimental research on mechanism and controlling of floor heave in deep soft rock roadway," *Journal of Mining and Safety Engineering*, vol. 34, no. 2, pp. 235–242, 2017.

[18] Z. Li, S. Li, and X. Zhao, "Floor heave controlling technology of deep soft rock roadway," *Applied Mechanics and Materials*, vol. 170-173, pp. 68–71, 2012.

[19] Y. Zhao, Y. Wang, W. Wang, W. Wan, and J. Tang, "Modeling of non-linear rheological behavior of hard rock using triaxial rheological experiment," *International Journal of Rock Mechanics and Mining Sciences*, vol. 93, pp. 66–75, 2017.

[20] S. Zhang, Z. Bei, and Y. F. Zhang, "The Causes Analysis and Control Measures about Rapid Floor Heave in Deep Mine," *Applied Mechanics and Materials*, vol. 94-96, pp. 786–790, 2011.

[21] P. W. Hao, H. L. Dong, Z. H. Liu, J. P. Li, and L. W. Jing, "Brief Analysis of Floor Grouting Method in Soft Rock Roadway Based on Engineering Materials and Engineering Mechanics," *Applied Mechanics and Materials*, vol. 345, pp. 442–446, 2013.

[22] Y. Chen, J. Bai, S. Yan, Y. Xu, X. Wang, and S. Ma, "Control mechanism and technique of floor heave with reinforcing solid coal side and floor corner in gob-side coal entry retaining," *International Journal of Mining Science and Technology*, vol. 22, no. 6, pp. 841–845, 2012.

[23] Y. Zhao, L. Zhang, W. Wang, J. Tang, H. Lin, and W. Wan, "Transient pulse test and morphological analysis of single rock fractures," *International Journal of Rock Mechanics and Mining Sciences*, vol. 91, pp. 139–154, 2017.

[24] Y. Zhao, L. Zhang, W. Wang, C. Pu, W. Wan, and J. Tang, "Cracking and Stress–Strain Behavior of Rock-Like Material Containing Two Flaws Under Uniaxial Compression," *Rock Mechanics and Rock Engineering*, vol. 49, no. 7, pp. 2665–2687, 2016.

[25] X. Fan, K. Li, H. Lai, Q. Zhao, and Z. Sun, "Experimental and numerical study of the failure behavior of intermittent rock joints subjected to direct shear load," *Advances in Civil Engineering*, vol. 2018, Article ID 4294501, 19 pages, 2018.

[26] Y. Wang, P. Guo, W. Ren et al., "Laboratory Investigation on Strength Characteristics of Expansive Soil Treated with Jute Fiber Reinforcement," *International Journal of Geomechanics*, vol. 17, no. 11, Article ID 04017101, 2017.